Carbon 109 (2016) 418–427

Contents lists available at ScienceDirect

Carbon

journal homepage: www.elsevier.com/locate/carbon

Orbital hybridization mechanism for the enhanced photoluminescence in edge-functionalized sp^2 carbon clusters

Byungkyun Kang [a], Yuri Choi [b], Byeong-Su Kim [a, b], Il Seung Youn [c], Geunsik Lee [a, *]

[a] Department of Chemistry, Ulsan National Institute of Science and Technology (UNIST), Ulsan 44919, South Korea
[b] Department of Energy Engineering, Ulsan National Institute of Science and Technology (UNIST), Ulsan 44919, South Korea
[c] Center for Superfunctional Materials, Department of Chemistry, UNIST, Ulsan 44919, South Korea

ARTICLE INFO

Article history:
Received 7 March 2016
Received in revised form
24 May 2016
Accepted 2 June 2016
Available online 3 June 2016

ABSTRACT

Using the first principles methods, we performed systematic study on the effect of edge-functional groups on the electronic energy levels and the optical properties of sp^2 carbon clusters. It is found that the intrinsic π and π^* orbitals are weakly altered by oxygen-bearing functional groups, but it is significantly disrupted by pyrrolic groups. Thereby the oscillator strength of the lowest-energy transition is found to be much stronger for the pyrrolic group functionalized cluster than for the carboxyl group. From our results being consistent with the experimental reports, we suggest that the photoluminescence enhancement is caused by a perturbation of the intrinsic frontier molecular orbitals by edge groups.

1. Introduction

Highly luminescent carbon dots (CDs) attract great interest owing to cost-effective synthesis and bio-compatible applications such as bioimaging [1,2] and biosensors [3]. They consist of a few-layer stack of defective graphene sheets with the lateral size less than 10 nm, where each layer is also regarded as a graphene quantum dots (GQDs). Various synthesis methods have been reported such as microwave heating [4], hydrothermal cutting of graphene sheets [5], and partial reduction of graphene oxide [6]. Different kinds of CDs have shown a similar UV–vis photoluminescence (PL) property, where the emission peak strongly depends on the excitation wavelength. A general principle is that radiatively-recombining electron-hole pairs need to be confined within a nanoscale sp^2 carbon cluster formed by edge or peripheral functional groups, leading to either a cluster or matrix shape, respectively. Although many studies have been devoted to figuring out microscopic details and to enhancing the PL quantum yield (QY), the origin of luminescence mechanism is not clearly understood yet.

In order to understand the luminescence mechanism we have to know the relaxation pathway of excited electrons. The absorbance of CDs typically exhibits a main peak around 260 nm and a shoulder around 320 nm. It has been suggested that the two peaks are due to transitions from a triplet ground state ($\sigma^1\pi^1$) of zigzag edge carbons to π^* of carbon core, which is supported by the observed pH dependence of PL intensity [5]. But there exists a wider consensus that the main peak is attributable to π-π^* transitions of C=C and the shoulder to n-π^* transitions of C=O [6–8]. Meanwhile there exists debate on a radiatively emissive orbital, that is the emission center of PL. Mainly two kinds of explanation have been reported, where it can be an intrinsic lowest-unoccupied molecular orbital (LUMO) or a defect state caused by functional groups. The former is ambiguously adopted to explain the excitation dependent PL that upon lowering the excitation energy (usually lower than n-π^* transition energy) the emission by larger dots is enhanced while the smaller one is suppressed, thus the emission wavelength red-shifts due to the decreasing highest-occupied molecular orbital (HOMO)-LUMO gap by the quantum confinement effect (QCE) [5]. It is further supported by an excitation-independent PL for monodisperse CDs [9]. On the other hand, clear evidences have been reported that edge functional groups introduce their own defect states as an emission center, thus affecting the PL property [10–16]. The emission peak red-shifts upon oxidation [11] and the intensity is enhanced significantly upon subsequent nitrogen doping [12], where both oxygen and nitrogen groups are suggested to be located at edges. It is claimed that such enhancement is caused by pyrrolic or graphitic forms of N [16]. More insight could be obtained from pump-probe experiments, where two distinct decaying rates were

* Corresponding author.
E-mail address: gslee@unist.ac.kr (G. Lee).

http://dx.doi.org/10.1016/j.carbon.2016.06.007
0008-6223/

identified and could be related to a radiative recombination and a trap to defect states [17–19].

Theoretical studies have shown that pyrrolic or pyridinic N-doping leads to a blue-shift of the PL emission according to their structural models without any indication of defect states behaving as an emission center [20,21], which is consistent with the experimental results on N-doped CDs [12]. But it should be noted that the results strongly-depend on the structure of sp^2 carbon cluster. It is necessary to have a deep insight without relying on a specific model. Thus, in this report, we study systematically the effect of various edge functional groups as well as chemical dopants on the electronic structure and resulting optical properties of the CDs by using the first principles method. It is suggested that the emission intensity is mainly decided by the strength of edge groups perturbing the intrinsic π and π^* frontier molecular orbitals (MOs).

2. Calculation details

Our calculations for the ground state are based on the density functional theory (DFT) with the local spin density approximation (LSDA) for the exchange correlation functional [22], which is denoted as LSDA/DFT. We use the pseudopotential plane wave basis package (VASP) with the projector augmented potentials, where the energy cutoff of 400 eV is used [23,24]. As shown in Fig. 1(a) or 1(b), we first consider an isolated GQD whose intrinsic form is modeled as a monolayer hexagon cluster with armchair or zigzag edges, where edge C is passivated by H. It represents polycyclic aromatic hydrocarbons or sp^2 domains embedded in a reduced graphene oxide matrix [6]. We use the supercell with 10 Å vacuum along each direction to decouple unphysical interaction between periodic images. All the structures are optimized until the atomic force is less than 0.01 eV/Å.

We consider various functional groups or dopants to study their effects on the electronic state, such as hydroxyl, carboxyl, carbonyl, pyrrolic, pyridinic N and graphitic N. Following the experimental observations [11,12], the chemical functional groups are introduced only at the edges, which can be related to groups residing at boundaries between sp^2 domains. For each type, the energy levels of frontier MOs are inspected with increasing the number of the edge group, where the HOMO-LUMO gap is a primarily interesting quantity. Among various configurations, we choose such dots with a sizable energy gap that we can associate with observed optical absorption and emission properties. The optical properties are studied by calculating the oscillator strength between the ground and excited states with the Gaussian09 package [25], where the time-dependent DFT (TD-DFT) method is used to describe excitation with the B3LYP hybrid functional for the exchange-correlation kernel, which is denoted as B3LYP/TD-DFT. The 6-31G* basis is used and the B3LYP parameters are 0.2 for the exact exchange, 0.8 for the LSDA exchange, 0.72 for the gradient correction of exchange, 0.81 and 0.19 for the non-local and local parts of the correlation energy [26,27]. For comparative purpose, the oscillator strength is also calculated between the ground state Hartree-Fock orbital and the singly excited configurations, which is denoted as HF/CIS. While two different packages, VASP and Gaussian09, are used for our computational convenience, we confirmed the qualitative agreement between the LSDA and B3LYP functionals for the ground state MO energy levels. The calculated oscillator strengths are broadened by Gaussian functions, in other words, the raw intensity I_0 at a transition energy E_0 is replaced by $(I/\pi^{1/2}\Gamma)\exp[-(E-E_0)^2/\Gamma^2]$ where we choose $\Gamma = 0.05$ eV to find the broadened peak value I. The emission intensity is calculated after we optimize the excited-state geometry.

3. Results and discussion

Our results are organized in three parts. First, the ground state electronic structures are shown for the pristine and chemically modified sp^2 carbon clusters, where the LSDA/DFT method is used, unless it is mentioned specifically. A monolayer GQD is adopted for a systematic study, and the effect of interlayer coupling (or aggregation effect) will be considered at the end. Second, the dots with a sizable energy gap are chosen and their oscillator strengths for the absorption and emission are given, which is calculated by the B3LYP/TD-DFT and HF/CIS methods. In the third part, we discuss our results on the basis of experimental reports.

3.1. Electronic structures

We consider three different cluster sizes for each of armchair and zigzag edge types, ranging from 0.6 to 1.4 nm in the radius (r). The smallest clusters correspond to $C_{42}H_{18}$ (armchair) and $C_{54}H_{18}$ (zigzag) as shown in Fig. 1(a) and (b), respectively. Fig. 1(c) and (d) show the calculated density of states (DOS) for different sizes of the armchair and.

zigzag types, where discrete energy levels and a smooth curve with their broadened contributions are shown together. As the size increases, the energy gap between HOMO and LUMO decreases due to the QCE. Also the HOMO and LUMO orbitals are characterized by the π bonding and antibonding states (π and π^*), respectively, which remains essentially the same irrespective of the edge type and the size, and each of them is doubly degenerate. From the probability distributions of HOMO and LUMO, shown in Fig. 1(e) and (f) for the smallest size, one can see that each of doubly degenerate LUMO (π^*-1, π^*-2) has one more node than its HOMO counterpart ($\pi-1$, $\pi-2$), respectively. Interestingly for the armchair case, there exists one more orbital near HOMO or LUMO with seemingly edge localized character, $\pi-3$ or π^*-3 in Fig. 1(e). In Fig. 1(c), the $\pi-3$ level appears a little lower than HOMO, and the π^*-3 almost overlaps with the LUMO level for $r = 0.6$ nm that gives higher intensity and for $r = 1.0$, 1.4 nm it appears a little higher than LUMO resulting in broader peaks.

It is known that the zigzag edge causes a peculiar state localized along the edge [28]. But it requires a sufficiently long zigzag edge. In our study, there is no edge localized state up to the largest dot (diameter 2.2 nm) considered here. Furthermore there have been theoretical reports that the armchair edge is 1.1 eV/atom more stable than the zigzag edge [29] and that even a sub-10 nm size, as observed experimentally, of the zigzag edge is almost free from the edge localized state [21]. Thus the peculiar edge state does not play an important role in current study and we focus on the π and π^* orbitals delocalized over the cluster. Since the delocalized character hardly depends on the edge type, we consider only the armchair edge type of the smallest cluster ($C_{42}H_{18}$) in the following investigation.

For edge oxidation and/or nitrogen doping on the armchair-edge cluster $C_{42}H_{18}$, we consider oxygen groups (carbonyl, carboxyl, hydroxyl group), nitrogen groups (pyridinic, pyrrolic, graphitic N) and a configuration with the two kinds coexisting. Fig. 2 shows the most energetically favorable configuration of oxygen and nitrogen atoms within the GQD according to our calculations. As for the well-known oxygen-bearing edge groups the planar shape is more favorable for carboxyl and hydroxyl groups. In case of a pyrrolic or pyridinic N group the configuration located at the outermost edge is favored, which is consistent with the experiments [11,12]. For the graphitic N, the most favorable site of N is a site next to the armchair edge. Also the coexisting configuration of carbonyl and graphitic N favors energetically the amide group,

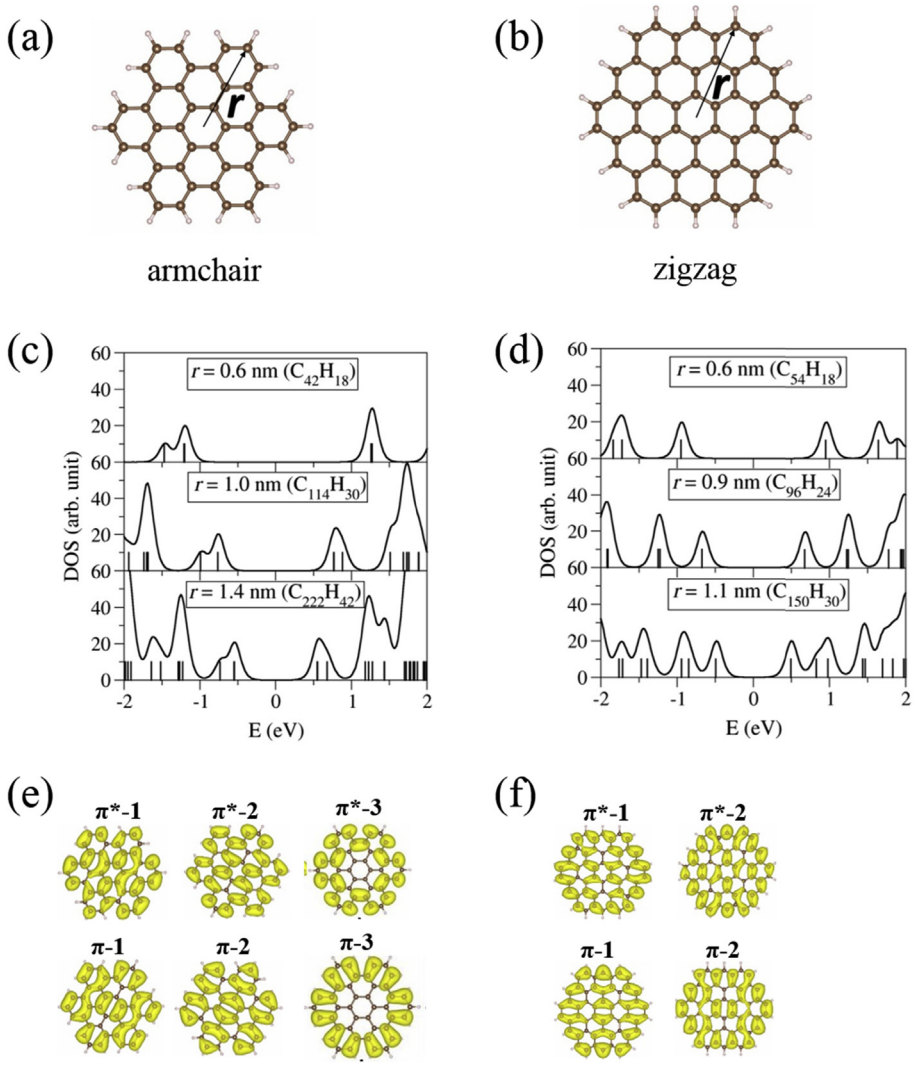

Fig. 1. GQD modeled by a monolayer hexagon cluster of sp^2 carbon with (a) the armchair or (b) zigzag edges, where the edge C atoms are passivated by H. The radius is about 0.6 nm for the armchair ($C_{42}H_{18}$) and zigzag ($C_{54}H_{18}$). (c) and (d) are the calculated density of states for the armchair and zigzag types, respectively, with the increasing cluster radius, where discrete energy levels and a smooth curve with their broadened contributions are shown together. (e) and (f) are the probability of two (or three for the armchair type) frontier MOs near HOMO ($\pi-1$, $\pi-2$, $\pi-3$) and LUMO (π^*-1, π^*-2, π^*-3) for the armchair and zigzag type clusters shown in (a) and (b), respectively. (A colour version of this figure can be viewed online.)

which is consistent with experimental reports [30,31], and we denote it as amide N hereafter as shown in Fig. 2. It is shown that the edge functionalization with respect to the pristine GQD is favored energetically, where we list the calculated reaction energy for each functionalization in Table 1. By assuming the gas-phase chemical environment, groups such as hydroxyl, carboxyl and amide N are highly likely to be formed, while N-containing groups are less likely.

Fig. 3 shows the DOS of the GQD after functionalization with each group as shown in Fig. 2, where we show the results by LSDA (VASP) and B3LYP (Gaussian09) functionals for qualitative comparison. For most cases, the HOMO and LUMO are remained occupied and empty, so that the π orbital system is electrically neutral. But for the carbonyl group electrons are withdrawn and for the graphitic N electrons are provided, which makes the π orbital system ionized positively and negatively, respectively. By mixing these two groups, we recover a neutral cluster, as shown for the amide N. Although the LSDA underestimates the band gap, the qualitative agreement between the two methods is good, so we rely on the LSDA results by VASP to make qualitative analysis on the ground state MOs.

In Fig. 4, we shows the probability distribution for frontier MOs of functionalized GQD, which can be compared to the pristine MOs shown in Fig. 1(e). One can see that the pyridinic N has a negligible role in changing the pristine MOs. It is because the N behaves as one π electron atom with a non-bonding pair. Also for the carboxyl case, the pristine MOs are almost unchanged, although a little hybridization between π^*-2 and O p orbitals can be seen for LUMO. For the hydroxyl case, the unoccupied orbitals are significantly different from those of the pristine dot, while the occupied orbitals remain almost the same. For the pyrrolic group, the modified π bond network perturbs the pristine MOs greatly, mainly unoccupied ones. In case of the carbonyl group, (SOMO+1), SOMO and (HOMO−1) should resemble the pristine HOMO ($\pi-1$ and $\pi-2$ in Fig. 1(e)) due to the withdrawn property if there is no hybridization effect, but a significant hybridization between the pristine MOs and O p orbital makes most MOs much different from the pristine MOs mainly due to a missing terminal hydrogen, otherwise it weakens

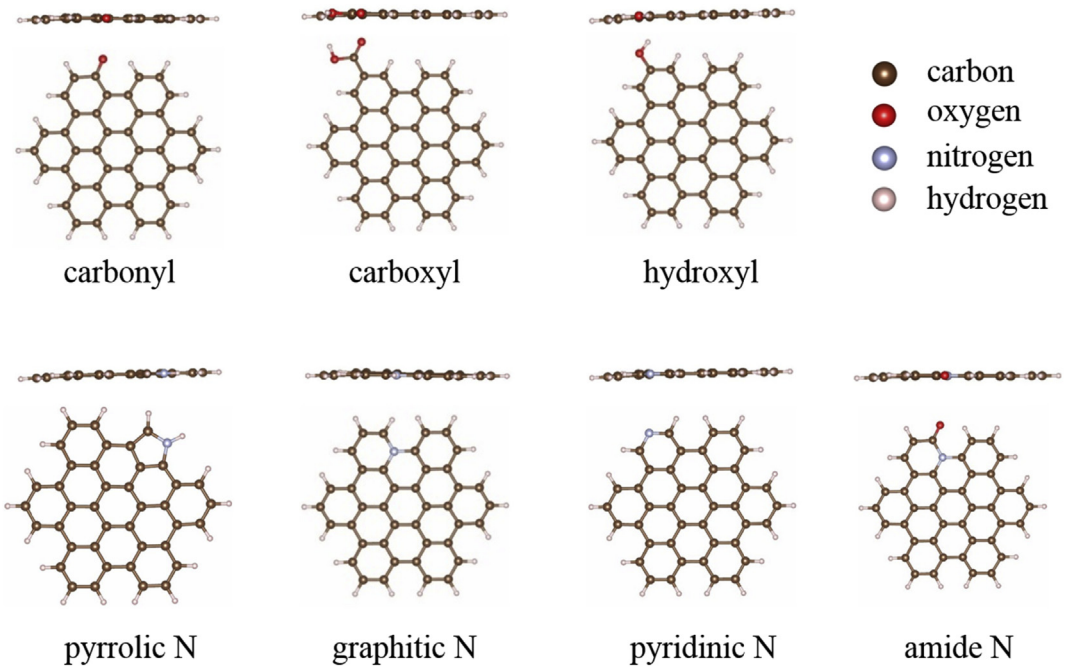

Fig. 2. Side and top views of the most stable GQD structure with an edge functionalization by each group (brown, carbon; red, oxygen; silver, nitrogen; bright gray, hydrogen).

Table 1
Calculated reaction energies (ΔE) by LSDA for the functionalized GQDs in Fig. 2.

Type	ΔE (eV)	Chemical reaction formula
Carbonyl	−0.407	$C_{42}H_{18} + 1/2O_2$ (g) → $C_{42}H_{17}O + 1/2H_2$ (g)
Carboxyl	−1.89	$C_{42}H_{18} + COOH$ (g) → $C_{42}H_{17}COOH + 1/2H_2$ (g)
Hydroxyl	−2.48	$C_{42}H_{18} + OH$ (g) → $C_{42}H_{17}OH + 1/2H_2$ (g)
Pyrrolic N	1.012	$C_{42}H_{18} + NH_3$ (g) → $C_{40}H_{16}NH + C_2H_4$ (g)
Graphitic N	0.599	$C_{42}H_{18} + NH_3$ (g) + $1/2H_2$ (g) → $C_{41}H_{18}N + CH_4$ (g)
Pyridinic N	0.027	$C_{42}H_{18} + NH_3$ (g) → $C_{41}H_{17}N + CH_4$ (g)
Amide N	−1.594	$C_{42}H_{18} + NH_3$ (g) + $1/2O_2$ (g) → $C_{41}H_{17}ON + CH_4$ (g)

the hybridization as seen in hydroxyl and carboxyl groups. For the graphitic N group, we see that SOMO, (SOMO+1) and (LUMO+1) are significantly different from the pristine LUMO (π^*-1, π^*-2 in Fig. 1(e)), because the nitrogen is an attractive defect as well as an electron-donating group. For the amide N, we see a significant modification for most MOs.

In this study, we focus on such groups that make the π orbital system neutral for simplicity, where the radical groups are discussed at the end with implication on optical transitions. So carboxyl, hydroxyl, pyrrolic, pyridinic N, and amide N groups are considered. For each of them, we increase the number of edge groups one by one, as shown in Fig. 5(a), and calculate the

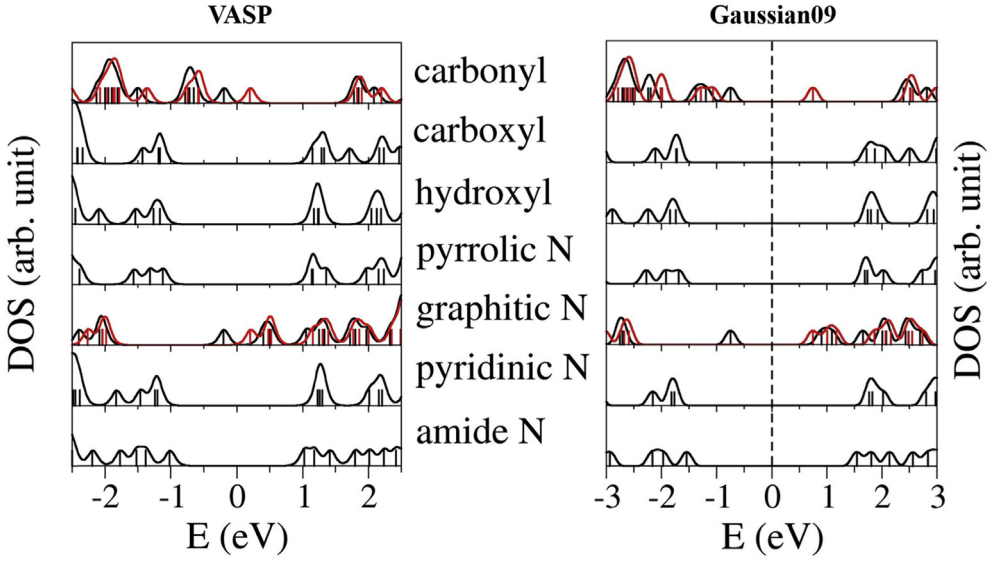

Fig. 3. Calculated density of states (DOS) for functionalized GQDs shown in Fig. 2 by (left) VASP with LSDA, (right) Gaussian09 with B3LYP. For the carbonyl and graphitic N cases, the black and red colors mean the spin up and down DOS, respectively, while for other cases DOS's by spin-restricted calculations are shown by the black color with the multiplicity two. (A colour version of this figure can be viewed online.)

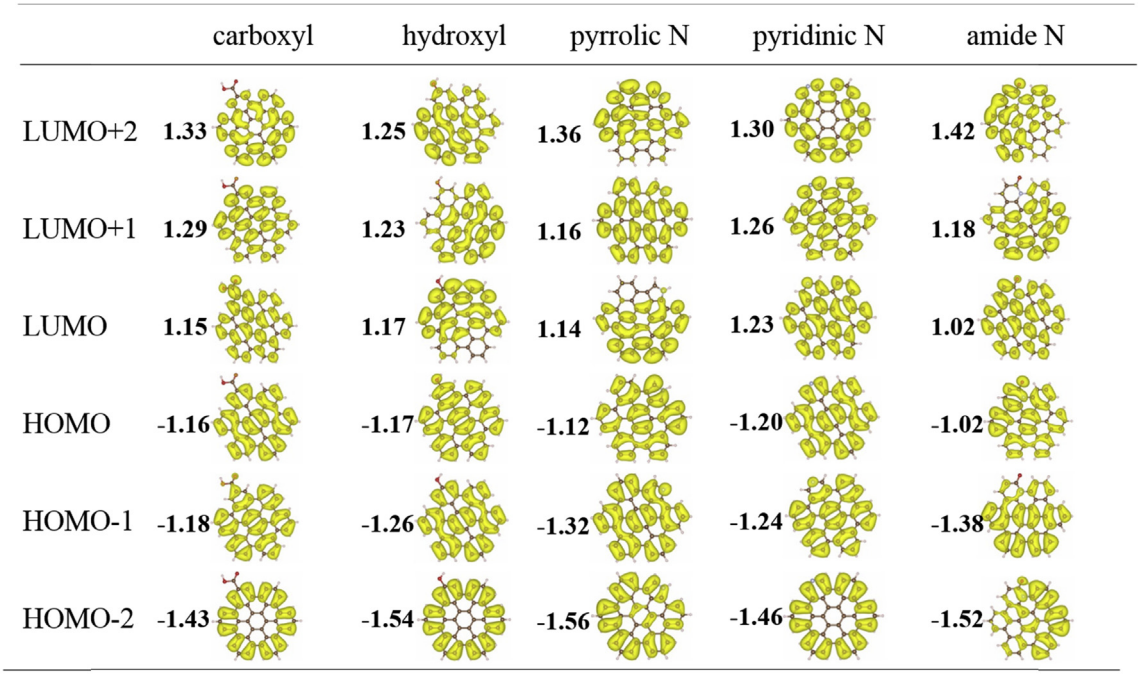

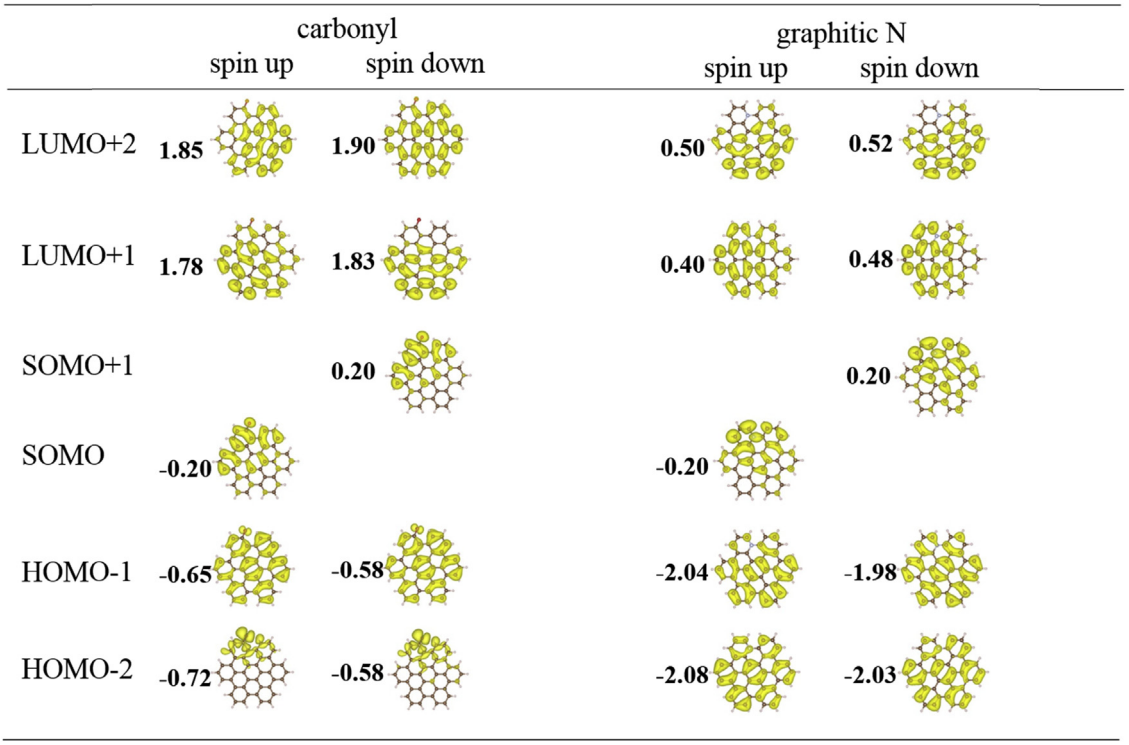

Fig. 4. Probability distribution and energy levels of MOs by LSDA for each functionalized GQD shown in Fig. 2. The spin multiplicity is two or one for the upper or lower panel, respectively. (A colour version of this figure can be viewed online.)

electronic structure to inspect the change of energy levels of the frontier MOs ($\pi-1$, $\pi-2$, $\pi-3$ and π^*-1, π^*-2, π^*-3). The results are shown in Fig. 5(b). We can see that pyrrolic N and amide N groups significantly change the energy levels as compared to the pristine case indicated by the horizontal dashed lines, while the others affect slightly. These are consistent with the trend of frontier MO disruption that we have seen for the GQD functionalized by a single group. Generally speaking, the magnitude of MO energy level modification will be proportional to the degree of edge functionalization with the ratio depending on the type of chemical groups. It will be shown in the following section that such perturbation dramatically affects optical absorption and emission properties.

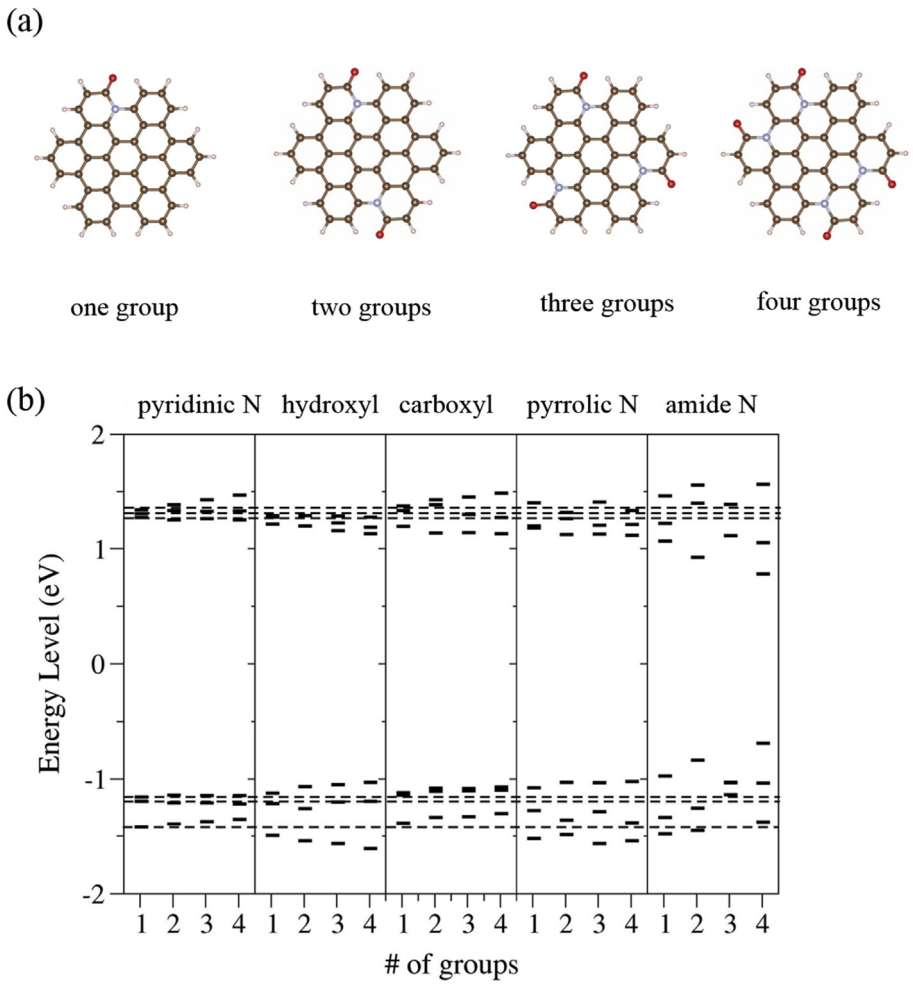

Fig. 5. (a) Atomic structures of GQDs after edge functionalization with one, two, three and four groups of amide N. The other functional group types follow the similar geometry. (b) Variations of frontier MO energy levels with increasing the number of edge groups for each functional type. The horizontal dashed lines denote the energy levels of the occupied $\pi-1$, $\pi-2$, $\pi-3$ and the unoccupied π^*-1, π^*-2, π^*-3 orbitals for the pristine dot as shown in Fig. 1(e). (A colour version of this figure can be viewed online.)

The size of experimental CDs (r ~ 10 nm) is much bigger than that of our model (r ~ 1.0 nm). Although our model is rather related to one of multiple sp^2 clusters residing in the CDs, we examine the dependence on the GQD size with fixing the number of edge groups, which effectively lowers the degree of edge functionalization. We choose the pyrrolic N and amide N, which are denoted as 'pN' and 'aN', respectively, with fixing the number of groups as four and consider both edge types, armchair and zigzag, thus they are denoted as pN-arm/zig and aN-arm/zig as depicted in Fig. 6(a). Our calculated results for three sizes are shown in Fig. 6(b). Overall, for both edge types, the energy levels approach to those of the pristine GQD as the size increase, where the amide N shows much slow variation. Our results are extrapolated to experimentally observed dot size r ~10 nm. In case of HOMO-LUMO gap, shown in Fig. 6(c), it is found that the pyrrolic N functionalization resembles the behavior of the pristine dot with almost zero gap at r ~ 10 nm (the vertical dashed line), that is the red line versus the black line. The zigzag type (dashed line) has a smaller gap than the armchair (solid line). Meanwhile the amide N shows a much slower decrease with increasing the size. We also analyze the level splitting of frontier MOs by choosing (LUMO+1) and LUMO, or HOMO and (HOMO−1), where the main conclusion would not be changed when one considers up to (LUMO+2) or (HOMO−2). As shown in Fig. 6(d) for the pyrrolic N, it approaches to zero for most cases except for the pN-arm LUMO splitting which shows much slower decrease than others. For aN-arm and aN-zig, not shown here, it approaches to zero for all cases.

3.2. Oscillator strengths

We choose three different groups to study the effect of edge functional groups on the optical transition probabilities, compared to the pristine sp^2 cluster. They are carboxyl group, pyrrolic N, and amide N, which seem to affect the frontier MOs significantly as observed from Figs. 4 and 5. For convenience, only two groups of the same kind at the opposite armchair edges are introduced, like two amide N groups of Fig. 5(a).

As shown in Fig. 1(c) ($C_{42}H_{18}$), the pristine cluster involves two degenerate ($\pi-1$, $\pi-2$) and $\pi-3$ orbitals below the Fermi level, and three (π^*-1, π^*-2 are degenerate, and π^*-3 almost overlaps) orbitals above. Based on the dipole transition matrix elements, a qualitative behavior on the optical transition probability can be understood in the following way, where both methods by TD-DFT and CIS involve singly excited configurations. Among nine possible transitions between filled and empty orbitals, the dipole matrix element is not vanishing only for two cases, (i) between one from $\pi-1$ or $\pi-2$ and the other from π^*-1 or π^*-2, (ii) between $\pi-3$ and π^*-3. Since the case (ii) involves higher transition energy

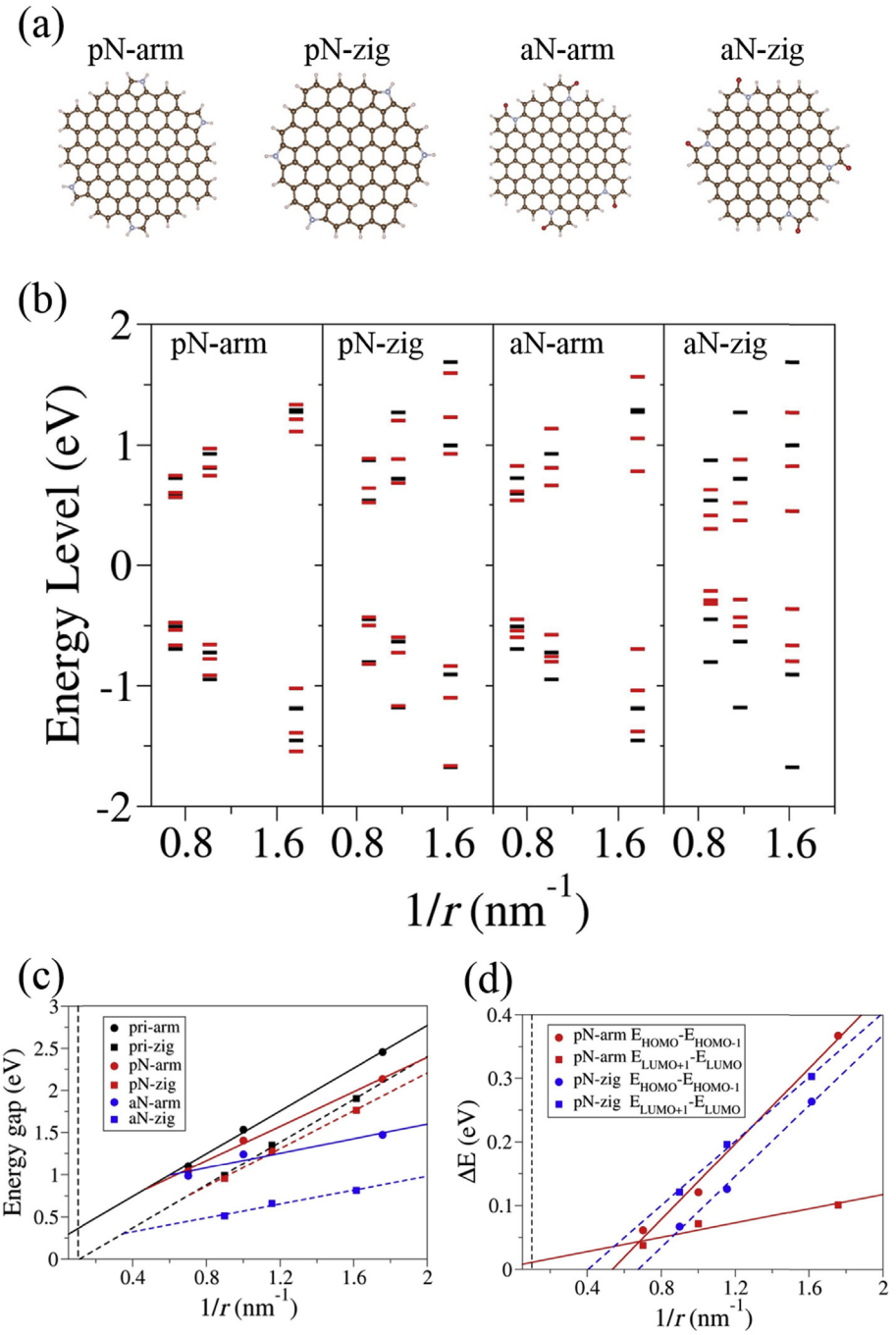

Fig. 6. LSDA results of frontier MO energy levels with varying the GQD size and edge type for each functionalization by pyrrolic N or amide N. (a) shows the structure of functionalized GQDs for the size r = 1.0 (armchair) or 0.9 (zigzag) nm, where four edge groups of each type are considered with a similar pattern for other sizes (e.g. Fig. 5(a) for the smallest armchair type). The notation is shortened such that pN-arm (pN-zig) refers to pyrrolic N functionalized dot for the armchair (zigzag) edge type and aN-arm (aN-zig) to amide N functionalized ones. (b) Three occupied or unoccupied MO energy levels as a function of the inverse of radius (1/r) for four cases listed in (a), where the black bars corresponds to the results for unfunctionalized dots. (c) HOMO-LUMO energy gap as a function of 1/r. (d) Energy level splitting between HOMO and (HOMO−1) or (LUMO+1) and LUMO a function of 1/r for the pN-arm and pN-zig cases. The lines are the guide to eye in (c) and (d), and the vertical dashed line corresponds to the experimental dot size (r = 10 nm). (A colour version of this figure can be viewed online.)

than the case (i), we can consider only four pairs from the case (i) for analyzing low energy transitions. Thus only four CIS bases can be considered in the pristine dot. According to our results by both methods, the pristine dot exhibits two low energy excitations (E1 and E2 in the inset of Fig. 7(a)) and one doubly degenerate high energy excitation (E3), where the transition probabilities from E0 to E1 and E2 are zero due to the symmetry. Hence the first nonzero absorption peak appears at 360 nm, associated with E3. Also the emission which is red-shifted by 22 nm relative to the E1 has zero probability (the red star in Fig. 7(a), Table 2).

Fig. 7(b), (c) and (d) show that once the cluster orbitals are perturbed by the edge groups, the originally vanishing oscillator strength becomes non-zero, where the trend is the same between B3LYP/TD-DFT and HF/CIS methods from Table 2. Overall peaks are

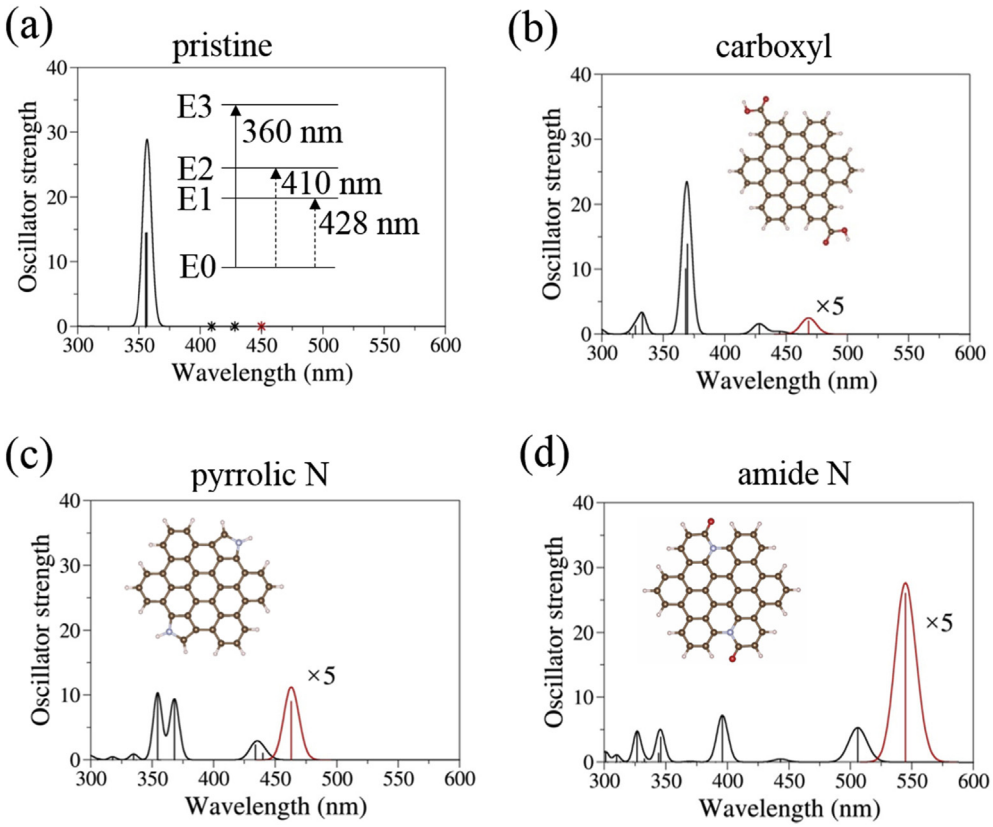

Fig. 7. Calculated oscillator strengths for the absorption (black) and the emission (red) by B3LYP/TD-DFT. Vertical lines are the raw intensities rescaled bigger for visibility, and they are broadened by Gaussian functions with a FWHM = 0.05 eV (see the text). (a) is the result for the pristine dot of Fig. 1(a), where three low-energy excitations (E1, E2, E3) from the ground state (E0) are illustrated in the inset (note E1 and E2 have zero intensity as marked by the stars in the main plot). (b), (c) and (d) are the results for the edge-functionalized dots by *two* groups of the given type with the structure shown in the inset. (A colour version of this figure can be viewed online.)

Table 2
Lowest-energy absorption (λ_{abs}) and emission (λ_{em}) wavelengths, and their oscillator strengths (f_{abs} and f_{em}), calculated by the B3LYP/TD-DFT method. Also the result by HF/CIS are shown in the parentheses. The pristine graphene quantum dot (GQD) is the smallest armchair-edge cluster, as shown in Fig. 1(a). For the other three GQDs, only two groups of the same kind are introduced at the edge as given in the insets of Fig. 7.

GQD type	λ_{abs} (nm)	f_{abs} (arb.)	λ_{em} (nm)	f_{em} (arb.)
Pristine	428 (323)	0.00 (0.00)	450 (339)	0.00 (0.00)
Carboxyl	445 (327)	0.021 (0.034)	468 (344)	0.025 (0.041)
Pyrrolic N	440 (331)	0.051 (0.259)	463 (349)	0.11 (0.318)
Amide N	506 (361)	0.27 (0.622)	545 (394)	0.28 (0.674)

more broadened, where carboxyl is the weakest and amide N strongest. As listed in Table 2, the lowest energy absorption probability (in arbitrary unit) is enhanced as 0.021, 0.051, 0.27 for carboxyl, pyrrolic N, amide N groups, respectively. It follows the same trend as the frontier MO disruptions (or energy level shifts) upon changing the type of edge groups (Fig. 4 and 5). As compared to the carboxyl case, it is enhanced by about four or nine times for the pyrrolic or amide N case. Interestingly, the emission slightly blue-shifts by the pyrrolic group (5 nm) and largely red-shifts by the amide N group (77 nm), compared to the carboxyl group. Also the hetero-functionalization with two kinds of groups is considered. From our calculation for the mixed carboxyl and pyrrolic N groups, higher intensities of the oscillator strengths are obtained as compared to those of the GQD with one kind of functional group (see Fig. S1 in Supplementary Information).

As one can see in Table 2, the absorption and emission wavelengths by the HF/CIS are much blue shifted by ~100 nm, as compared to those by the B3LYP/TD-DFT. The main reason for larger excitation energy by HF/CIS is that (i) the ground state orbitals are used in describing electronic excitations, which will differ from one-electron excited state orbitals, (ii) the correlation effect is not treated property due to the limitation of single excited configurations whose determinants are orthogonal to the ground state one [32].

3.3. Discussion

D. Pan et al. observed that blue luminescence at ~430 nm occurs when oxidized graphene sheets are reduced hydrothermally to form CDs with residual carboxyl groups at edges [5]. The similar result was reported for oxidized CDs obtained by different procedures [6,33]. The emission was primarily attributed to the transition from LUMO to HOMO orbitals of the CDs whose size varies from 3 to 10 nm [6,33]. According to our results, it is predicted that the emissive transition appears at $\lambda_{em} = 468$ nm for the carboxyl-functionalized cluster (Table 1), which is comparable to the experimental result but the GQD diameter is 1.2 nm in our model. Assuming the λ_{em} dominated by the QCE, where the emission red-shifts as the size becomes larger, it might be suggested that each layer of the CDs consists of multiple sp^2 domains as small as 1 nm, as mentioned in G. Eda et al. [6].

Further doping with nitrogen is known to enhance the QY [12,15,16]. In a good agreement with what has been suggested about nitrogen species, our study shows that the enhancement is mainly caused by the pyrrolic groups. Meanwhile, from Table 1 or

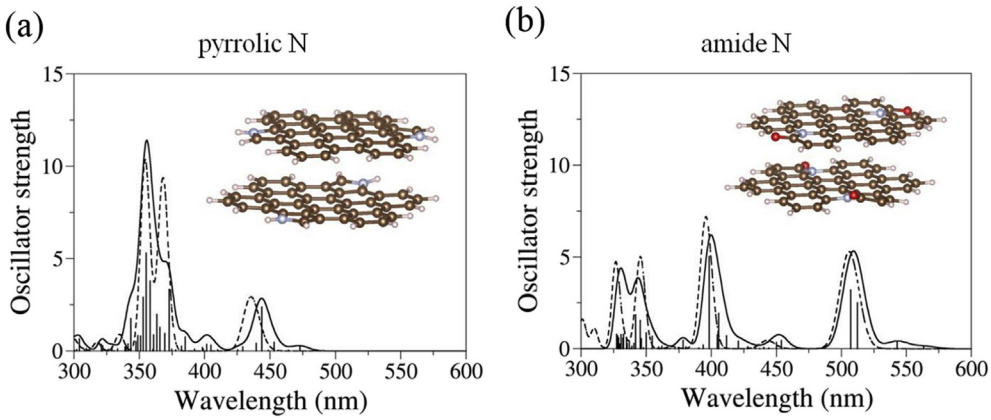

Fig. 8. Calculated absorption oscillator strengths for the AB stacked bilayer of GQDs with edge-functionalization by four groups of (a) pyrrolic N, (b) amide N. The dashed line is the result for the monolayer case, which is the same as what is shown in Fig. 6(c) and (d). The broadening scheme of raw vertical lines is the same as that in Fig. 6. (A colour version of this figure can be viewed online.)

Fig. 6, the two kinds of nitrogen groups (pyrrolic and amide N) show a significantly different emission wavelength, i.e. 82 nm red-shifted emission for the amide N than the pyrrolic N. Since the experiments do not show a significant variation in the emission wavelength before and after doping an oxidized CDs with nitrogen [12,15,16], it is likely that the N-doped oxidized CDs do not have a significant contribution by the amide N, but the pyrrolic groups play a major role in the enhancement. If the amide N was dominant, the PL could be further enhanced at a longer wavelength. But questions are still remained whether a functional group other than those considered here plays an important role in the emission and whether the π^* to π transition, not via defect states, is a plausible PL mechanism.

Experimental samples consist of multilayers of GQDs. In general the radiative transition is suppressed upon aggregation. We study the inter-layer coupling effect by considering a bilayer stacked GQDs. Fig. 8 shows the calculated oscillator strength for the AB-stacked bilayer of the pyrrolic (Fig. 8(a)) or amide N (Fig. 8(b)) modified GQDs. Compared to the result of the monolayer GQD, that is shown by the dashed line, overall shape is broadened with additional small peaks at lower energy than the main peak characterized by the monolayer HOMO-LUMO gap. In addition to the main transition, it would induce lower energy excitations or relaxations, thus making the non-radiative transitions possible assisted mainly by atomic vibrations. Thus the emissive transition will be weakened, compared to the single layer case. Conversely, it implies that exfoliation of multilayers will increase the QY in the experiments. Meanwhile our edge groups listed in Fig. 2 can induce defective emission centers. For example, in case of the open shell, such as a single group of carbonyl or graphitic N, the SOMO or (SOMO+1) causes very weak absorption peaks at much lower energies than 500 nm, around 1000 nm (see Fig. S2 in Supplementary Information). This could suppress the QY or make the non-radiative transition possible.

4. Conclusion

We have studied systematically the effect of edge-functional groups on the electronic energy levels of CDs and how it affects the optical properties. It is found that the intrinsic π and π^* orbitals are weakly altered by oxygen-bearing groups (carboxyl, hydroxyl), but it is significantly disrupted by nitrogen groups (pyrrolic, amide N). Thereby the oscillator strength of the lowest-energy transition is found to be much stronger for the pyrrolic group functionalized cluster than for the carboxyl group, which is consistent with the experimental results. It is also predicted that an amide N group would give further PL enhancement. Through comparison with reported experimental results, we provide an insight toward better understanding of the optical properties of CDs.

Acknowledgements

This work was supported by the National Research Foundation of Korea (2015R1C1A1A01055922, 2014R1A2A1A11052829).

Appendix A. Supplementary data

Supplementary data related to this article can be found at http://dx.doi.org/10.1016/j.carbon.2016.06.007.

References

[1] Y. Choi, S. Kim, M.H. Choi, S.R. Ryoo, J. Park, D.H. Min, et al., Highly biocompatible carbon nanodots for simultaneous bioimaging and targeted photodynamic therapy in vitro and in vivo, Adv. Funct. Mater 24 (37) (2014) 5781–5789.
[2] S.T. Yang, L. Cao, P.G. Luo, F. Lu, X. Wang, H. Wang, et al., Carbon dots for optical imaging in vivo, J. Am. Chem. Soc. 131 (32) (2009) 11308–11309.
[3] J. Zhao, G. Chen, L. Zhu, G. Li, Graphene quantum dots-based platform for the fabrication of electrochemical biosensors, Electrochem Commun. 13 (1) (2011) 31–33.
[4] H. Zhu, X. Wang, Y. Li, Z. Wang, F. Yang, X. Yang, Microwave synthesis of fluorescent carbon nanoparticles with electrochemiluminescence properties, Chem. Commun. 34 (2009) 5118–5120.
[5] D. Pan, J. Zhang, Z. Li, M. Wu, Hydrothermal route for cutting graphenes sheets into blue-luminescent graphene quantum dots, Adv. Mater 22 (6) (2010) 734–738.
[6] G. Eda, Y.Y. Lin, C. Mattevi, H. Yamaguchi, H.A. Chen, I.S. Chen, et al., Blue photoluminescence from chemically derived graphene oxide, Adv. Mater 22 (4) (2010) 505–509.
[7] M. Zhang, L. Bai, W. Shang, W. Xie, H. Ma, Y. Fu, et al., Facile synthesis of water-soluble, highly fluorescent graphene quantum dots as a robust biological label for stem cells, J. Mater Chem. 22 (15) (2012) 7461–7467.
[8] Y. Wang, S. Kalytchuk, Y. Zhang, H. Shi, S.V. Kershaw, A.L. Rogach, Thickness-dependent full-color emission tunability in a flexible carbon dot ionogel, J. Phys. Chem. Lett. 5 (8) (2014) 1412–1420.
[9] Q. Xue, H. Huang, L. Wang, Z. Chen, M. Wu, Z. Li, et al., Nearly monodisperse graphene quantum dots fabricated by amine-assisted cutting and ultrafiltration, Nanoscale 5 (24) (2013) 12098–12103.
[10] L. Wang, S.J. Zhu, H.Y. Wang, S.N. Qu, Y.L. Zhang, J.H. Zhang, et al., Common origin of green luminescence in carbon nanodots and graphene quantum dots, ACS Nano 8 (3) (2014) 2541–2547.
[11] L. Bao, Z.L. Zhang, Z.Q. Tian, L. Zhang, C. Liu, Y. Lin, et al., Electrochemical tuning of luminescent carbon nanodots: from preparation to luminescence mechanism, Adv. Mater 23 (48) (2011) 5801–5806.
[12] Y. Li, Y. Zhao, H. Cheng, Y. Hu, G. Shi, L. Dai, et al., Nitrogen-doped graphene quantum dots with oxygen-rich functional groups, J. Am. Chem. Soc. 134 (1)

(2012) 15–18.
[13] Y.Q. Zhang, D.K. Ma, Y. Zhuang, X. Zhang, W. Chen, L.L. Hong, et al., One-pot synthesis of n-doped carbon dots with tunable luminescence properties, J. Mater Chem. 22 (33) (2012) 16714–16718.
[14] Z.L. Wu, P. Zhang, M.X. Gao, C.F. Liu, W. Wang, F. Leng, et al., One-pot hydrothermal synthesis of highly luminescent nitrogen-doped amphoteric carbon dots for bioimaging from bombyx mori silk – natural proteins, J. Mater Chem. B 1 (22) (2013) 2868–2873.
[15] C. Hu, Y. Liu, Y. Yang, J. Cui, Z. Huang, Y. Wang, et al., One-step preparation of nitrogen-doped graphene quantum dots from oxidized debris of graphene oxide, J. Mater Chem. B 1 (1) (2013) 39–42.
[16] Y. Dai, H. Long, X. Wang, Y. Wang, Q. Gu, W. Jiang, et al., Versatile graphene quantum dots with tunable nitrogen doping, Part Part Syst. Char. 31 (5) (2014) 597–604.
[17] L. Wang, S.J. Zhu, H.Y. Wang, Y.F. Wang, Y.W. Hao, J.H. Zhang, et al., Unraveling bright molecule-like state and dark intrinsic state in green-fluorescence graphene quantum dots via ultrafast spectroscopy, Adv. Opt. Mater 1 (3) (2013) 264–271.
[18] Q. Xu, Q. Zhou, Z. Hua, Q. Xue, C. Zhang, X. Wang, et al., Single-particle spectroscopic measurements of fluorescent graphene quantum dots, ACS Nano 7 (12) (2013) 10654–10661.
[19] S. Zhu, L. Wang, B. Li, Y. Song, X. Zhao, G. Zhang, et al., Investigation of photoluminescence mechanism of graphene quantum dots and evaluation of their assembly into polymer dots, Carbon 77 (2014) 462–472.
[20] V. Strauss, J. Margraf, C. Dolle, B. Butz, T. Nacken, J. Walter, et al., Carbon nanodots: toward a comprehensive understanding of their photoluminescence, J. Am. Chem. Soc. 136 (49) (2014) 17308–17316.
[21] M.A. Sk, A. Ananthanarayanan, L. Huang, K.H. Lim, P. Chen, Revealing the tunable photoluminescence properties of graphene quantum dots, J. Mater Chem. C 2 (34) (2014) 6954–6960.
[22] J.P. Perdew, A. Zunger, Self-interaction correction to density-functional approximations for many-electron systems, Phys. Rev. B 23 (1) (1981) 5048.
[23] G. Kresse, J. Furthmüller, Efficient iterative schemes for ab initio total-energy calculations using a plane-wave basis set, Phys. Rev. B 54 (16) (1996) 11169–11186.
[24] G. Kresse, D. Joubert, From ultrasoft pseudopotentials to the projector augmented-wave method, Phys. Rev. B 59 (3) (1996) 1758–1775.
[25] M.J. Frisch, G.W. Trucks, H.B. Schlegel, G.E. Scuseria, M.A. Robb, J.R. Cheeseman, et al., Gaussian 09, revision B.01, Gaussian, Inc., Wallingford CT, 2009.
[26] C. Lee, W. Yang, R.G. Parr, Development of the Colle-Salvetti correlation-energy formula into a functional of the electron density, Phys. Rev. B 37 (2) (1988) 785–789.
[27] A.D. Becke, Density-functional thermochemistry. III. The role of exact exchange, J. Chem. Phys. 98 (7) (1993) 5648–5652.
[28] G. Lee, K. Cho, Electronic structures of zigzag graphene nanoribbons with edge hydrogenation and oxidation, Phys. Rev. B 79 (16) (2009) 165440.
[29] C. Hyun, J. Yun, W.J. Cho, C.W. Myung, J. Park, G. Lee, et al., Graphene edges and beyond: temperature-driven structures and electromagnetic properties, ACS Nano 9 (5) (2015) 4669–4674.
[30] Z.A. Qiao, Y. Wang, Y. Gao, H. Li, T. Dai, Y. Liua, et al., Commercially activated carbon as the source for producing multicolor photoluminescent carbon dots by chemical oxidation, Chem. Commun. 46 (2010) 8812–8814.
[31] X. Zhai, P. Zhang, C. Liu, T. Bai, W. Li, L. Daic, et al., Highly luminescent carbon nanodots by microwave-assisted pyrolysis, Chem. Commun. 48 (64) (2012) 7955–7957.
[32] A. Dreuw, M. Head-Gordon, Single-reference ab initio methods for the calculation of excited states of large molecules, Chem. Rev. 105 (11) (2005) 4009–4037.
[33] J. Peng, W. Gao, B.K. Gupta, Z. Liu, R. Romero-Aburto, L. Ge, et al., Graphene quantum dots derived from carbon fibers, Nano Lett. 12 (2) (2012) 844–849.